Journal of The Electrochemical Society, **153** (10) C701-C706 (2006)
0013-4651/2006/153(10)/C701/6/$20.00 © The Electrochemical Society

ALD and Characterization of Aluminum Oxide Deposited on Si(100) using Tris(diethylamino) Aluminum and Water Vapor

Rajesh Katamreddy,[a,b] Ronald Inman,[a,*] Gregory Jursich,[a] Axel Soulet,[a] and Christos Takoudis[b,*,z]

[a]*American Air Liquide, Chicago Research Center, Countryside, Illinois 60525, USA*
[b]*Departments of Chemical Engineering and Bioengineering, University of Illinois at Chicago, Chicago, Illinois 60607, USA*

A nonpyrophoric, oxygen-free, halogen-free tris(diethylamino) aluminum (TDEAA) precursor was used for atomic layer deposition (ALD) of aluminum oxide on Si(100). ALD of aluminum oxide using TDEAA and water was found to be self-limiting with respect to both reactants. The temperature window for ALD in the hotwall reactor used was found to be between 200 and 400°C. The ALD rate was 1.4 Å/cycle at optimum conditions. Fourier transform infrared (FTIR) analyses indicated negligible interfacial SiO_2 growth during deposition. Both FTIR spectra and transmission electron micrographs showed the ALD aluminum oxide to be amorphous. Also, FTIR and X-ray photoelectron spectral (XPS) analyses showed negligible carbon and nitrogen ($<1\%$ atomic) contamination in the film. Z-contrast images and electron energy loss spectra showed uniform aluminum oxide film with an abrupt interface with Si. XPS analysis revealed aluminum oxide film to be stoichiometric with no detectable Al–Al cluster formation. Also, XP spectra showed no silicate formation at the interface of as-deposited alumina films.
© 2006 The Electrochemical Society. [DOI: 10.1149/1.2239258] All rights reserved.

Manuscript submitted March 14, 2006; revised manuscript received May 8, 2006. Available electronically August 4, 2006.

In future minimization of transistor devices, alternative high-dielectric-constant materials are needed to replace SiO_2 and its first-generation replacement material, silicon oxynitride.[1] Among the potential replacement materials, aluminum oxide has gained considerable interest. Aluminum oxide has many favorable properties like high bandgap[2,3] and thermal stability on Si[4] and it remains amorphous after high-temperature annealing for future silica replacement. However, it has a relatively low dielectric constant (~ 9)[5] and this makes it a short-term replacement material. In order to take advantage of the material benefits of aluminum oxide without the electrical disadvantage of low dielectric constant, a combination film of aluminum oxide with higher dielectric metal oxides is potentially a better, longer term replacement material. Of possible combinations with aluminum oxide, hafnium oxide and zirconium oxide are currently being investigated.[2,6-8] Some recent studies have reported improvement in crystallization temperature and interfacial stability by mixing aluminum oxide with hafnium oxide.[9,10] It has been widely assumed that a thin silicon oxide interfacial layer is required for excellent electrical properties, but the presence of a silicon oxide interfacial layer places another constraint on the physical thickness. Aluminum oxide films also have a significant market in capacitor and some nonintegrated circuit applications like magnetic heads.

Atomic layer deposition (ALD) is being increasingly used to grow thin films in the microelectronics industry. The ALD process involves a sequential alternating series of gas-surface reaction under surface saturation conditions. Precursor and oxidizer are pulsed, alternately separated by inert gas purging periods to prevent gas phase reactions and obtain self-limiting film deposition. Each cycle results in a submonolayer growth of the required film. ALD has attractive features like excellent uniformity, conformality, and submonolayer thickness control.[11]

ALD of Al_2O_3 films is commonly performed today using alkyl aluminum or alkyl aluminum hydride as Al source.[12-15] One of the disadvantages of alkyl aluminum precursors such as tri-methyl aluminum (TMA) is that they are pyrophoric, which requires special handling and storage precautions. In addition to pyrophoricity, TMA contains aluminum–carbon (Al–C) bonds, which may result in undesirable carbon incorporation in the film. Aluminum isopropoxide has also been used as precursor to deposit aluminum oxide.[16] However, this compound polymerizes easily and thus exists as a mixture of polymers or oligomers. Each polymer or oligomer has a different vapor pressure. As a result, the vapor pressure of this precursor is unpredictable and difficult to control. Aluminum 2-ethyhexanoate has also been demonstrated as a precursor for Al_2O_3 deposition, but its low vapor pressure results in low deposition rates, which limits its usefulness.[17] In addition, many of the nonpyrophoric candidates contain aluminum–oxygen (Al–O) bonds. These bonds are quite strong (122 kcal/mol) compared to aluminum–nitrogen (Al–N) bonds (71 kcal/mol), which gives alkyl amino aluminum precursors a clear advantage in the energetics of reaction.

The advantage in using higher alkyl amino aluminum compounds, such as diethyl or higher carbon chain amino aluminum compounds, rather than methyl amino aluminum compounds, is that the higher alkyl amino aluminum compounds are less susceptible to self degradation by oligomerization. Another advantage of using diethyl amino compounds is that, unlike methyl amino aluminum compounds, the diethyl amino aluminum compound exists as a liquid. Thus, it is easier to control and provides more consistent delivery to the deposition tool. In this work, we present a nonpyrophoric, halogen-free, oxygen-free precursor, tris(diethylamino) aluminum (TDEAA; U.S. Pat. Appl. 20050003662), which along with water is used for ALD of aluminum oxide. Self-limiting kinetics for both precursor and water half-cycles are shown. Effects of temperature on deposition rate and on the vapor pressure of the novel precursor are also presented. Further, aluminum oxide film and its interface with Si are analyzed using Fourier transform infrared spectroscopy (FTIR), X-ray photoelectron spectroscopy (XPS), and scanning transmission electron microscopy (STEM)/electron energy loss spectroscopy (EELS) techniques.

Experimental

Aluminum oxide thin films were deposited using tris(diethylamino) aluminum precursor and water as oxidizing agent on p-doped 1×1 in. Si(100) substrates in a hot wall tube reactor with a resistive heater coil. Prior to deposition, Si wafers were cleaned by RCA standard cleaning (SC-1) to remove organic contaminants and particulates, followed by 1% HF dip for 40 s. Each of the two steps was followed by thorough deionized (DI) water rinse and drying in N_2. This cleaning procedure left approximately 10 Å of native oxide on the surface.

The reactor consists of a high-purity quartz tube (38 mm diam $\times$ 480 mm long) with an aluminum block serving as a substrate

* Electrochemical Society Active Member.
z E-mail: takoudis@uic.edu

Downloaded 12 Jul 2008 to 128.248.155.225. Redistribution subject to ECS license or copyright; see http://www.ecsdl.org/terms_use.jsp

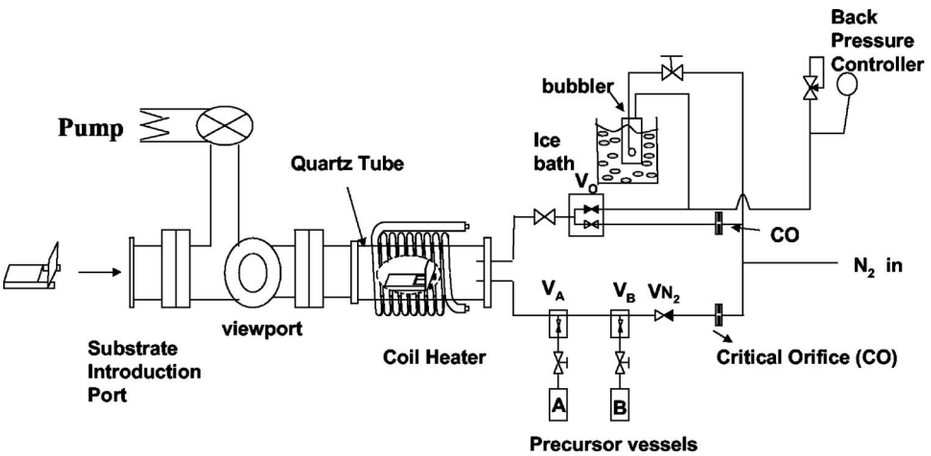

Figure 1. Schematic of the ALD reactor used for aluminum oxide deposition on Si(100).

holder, as shown in Fig. 1. Silicon substrate sits in the groove on the aluminum block with the deposition surface being perpendicular to reactant flow. The reactor can be heated to 650°C, although typically depositions are done at 150–450°C. The temperature of the heated zone during deposition (and called "reactor temperature" from now on) was measured using a type-K thermocouple glued to the outside surface of the quartz tube and controlled using a proportional integral differential (PID) controller (Omega CN 9000). PID settings were optimized so that the temperature control was obtained within ±1°C of the set point. The temperature uniformity of the heated zone was measured by inserting a thin type-K thermocouple probe along the cylindrical axis of the reactor and measuring temperature with this probe as it was positioned at different distances along the zone. Within the length of heater coil, the thermocouple measurements showed less than 2% deviation over a 10 cm distance. The temperature measured inside the reactor was about 25°C lower than the temperature measured on the outside surface of the quartz tube in the 200–450°C range. The inside temperature likely represents the deposition surface temperature.

The ALD precursor was introduced into the reactor by pulsing vaporized precursor using nitrogen carrier gas. The precursor vessel was heated in a copper block and the temperature was controlled using a PID controller. The precursor was introduced using a simple pulsing sequence. First, the precursor container and manifold leg were filled with carrier gas typically for 1 s and then the carrier gas line was closed using the pneumatic valve V_{N_2} (Fig. 1) to empty the vaporized precursor diluted in carrier gas into the reactor. This cycle of filling carrier gas in the precursor vessel and subsequent evacuation into the reactor is called a precursor "plug." We repeated this plug to inject the total amount of precursor needed for an ALD cycle (typically in an ALD reactor, the amount of precursor injected is controlled by changing the pulse time). The use of plugs enhances mass transport by increasing the pressure gradient between the precursor vessel and the reactor. A similar kind of precursor injection has been reported earlier by Becker et al.[18] This step is followed by a nitrogen purge to remove physisorbed precursor. The temperature of the precursor manifold was independently controlled typically 10–15°C above the reservoir temperature in order to prevent precursor condensation. The moisture reagent was introduced into the reactor as a diluted mixture with nitrogen carrier gas. The mixture originated from a separate manifold as indicated in Fig. 1. The source for moisture was ultrapure deionized water which was delivered from a bubbler maintained near 0°C using an ice bath and nitrogen carrier gas. The moisture pulse was then followed by a nitrogen purge to remove physisorbed water. This cycle was repeated as many times as desired to grow thicker films.

The vapor pressure of the TDEAA was measured directly using a heated vacuum manifold equipped with a heated capacitance manometer. The pressure gauge and manifold were both temperature controlled. The precursor vessel can be cooled to as low as 77 K using a liquid nitrogen bath or heated with a resistive band heater in conjunction with a PID temperature controller. The combination of both heating and cooling was used to induce freeze–pump–thaw cycles, thereby discriminating between true precursor vapor pressure and artificially high vapor pressure from possible liquid degassing and degradation by-products.

In this study film thicknesses were measured using spectral ellipsometry (J. A. Woollam Co., Inc., model M-44) and reflectometry (Mission Peak Optics, Inc., MP100-S). FTIR spectroscopy (Nicolet, Magna-IR 560) was used in the normal transmission mode over the wave number range of 4000–400 cm^{-1}. Spectra of cleaned wafers prior to deposition were used for background subtraction of the spectra of postdeposition wafers. Such subtraction spectra provide information about the deposited film and changes at the interface during deposition without the spectral features of the substrate itself.

A JEOL 2010F TEM/STEM was used which has a Schottky field emission gun source and operated at 200 kV with a JEOL annular dark-field detector and postcolumn Gatan imaging filter. The Gatan imaging filter was used in spectroscopy mode to collect EEL spectra.[19] The lens conditions in the microscope were defined for a probe size of 0.2 nm, with a convergence angle of 13 mrad and a collection angle of 52 mrad. As the two techniques do not interfere, Z-contrast images could be used to position the electron probe at the desired spot in the sample to acquire EEL spectra.[20,21] The accumulation time of each spectrum acquisition was 0.1 s for low-loss spectrum and 5.0 s for core-loss spectrum. Energy loss spectra at 0–100 eV (low loss) were measured to give information about the valence electrons of the specimen. Along with these low-loss spectra, O K-edge spectra in the 550–600 eV range were also measured to examine other core electron states within the specimen.

The Kratos AXIS-165 surface analysis system equipped with a monochromatic Al Kα and a concentric hemispherical analyzer coupled with a charge neutralizer was used for XPS analysis of 4.5 nm aluminum oxide on Si substrate. The analyzer was operated at pass energy of 40 eV to record Al 2p and Si 2p core-level spectra and the takeoff angle was 90°.

Results and Discussion

TDEAA vapor pressure dependence on temperature.— One of the most critical thermal parameters of precursors is its vapor pressure as a function of temperature. Sufficient precursor vapor density is needed to allow adequate deposition rates and yet care is needed in not overheating precursor beyond the temperature of self-decomposition. Thus, from knowledge of thermal temperature limit of the precursor prior to decomposition and its vapor pressure, one can assess the maximum range of permissible precursor reservoir temperature for the process with a given precursor.

Downloaded 12 Jul 2008 to 128.248.155.225. Redistribution subject to ECS license or copyright; see http://www.ecsdl.org/terms_use.jsp

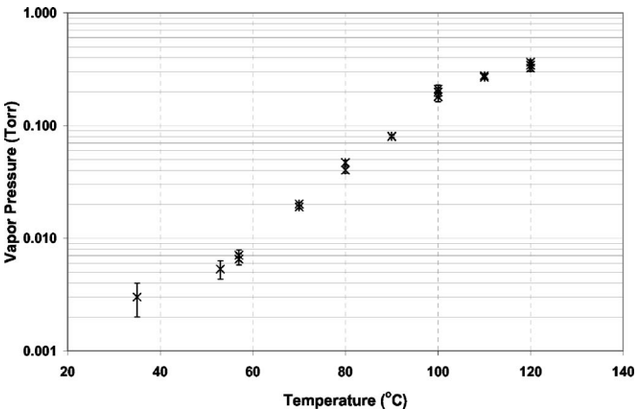

Figure 2. TDEAA vapor pressure vs temperature (semilog plot) showing exponential increase in vapor pressure with temperature.

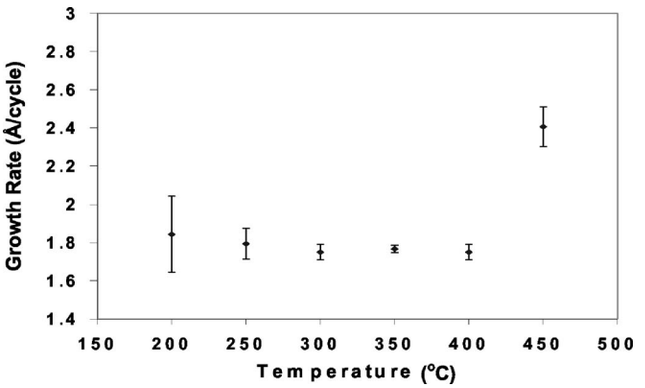

Figure 4. Deposition rate (Å/cycle) of aluminum oxide on Si(100) for five plugs vs reactor temperature. Error bars indicate film uniformity across the wafer sample.

In the vapor pressure measurements, the precursor vessel is heated to the required temperature and the vapor pressure is measured from an evacuated heated manifold. The measurements are considered reliable only after the pressure in the manifold is stable over time. For each temperature, the measurements are repeated to make sure that results are reproducible and to verify that decomposition by-products are not influencing the vapor pressure measurements. In Fig. 2, the TDEAA precursor vapor pressure is given as a function of temperature (semi-log plot). TDEAA vapor pressure appears to have exponential dependence on temperature with highest rate of increase between 55 and 105°C. For our ALD of aluminum oxide with TDEAA precursor, the temperature of the precursor vessel was maintained at 105°C.

ALD aluminum oxide: Precursor plugs.— Figure 3 shows the effect of the number of precursor plugs on the growth rate of aluminum oxide with error bars representing variation of thickness measurements across the substrate. The graph is similar to a typical ALD precursor pulse effect on growth rate which indicates that the discontinuous (plugs) method of precursor delivery works as well as continuous precursor injection for ALD.[12,13,18] From Figure 3, the growth rate seems to level off to ~1.4 Å/cycle at about five plugs of precursor with no variation of uniformity within the ALD regime where the deposition surface is saturated with precursor molecules. Further increase in number of plugs does not affect the growth rate as the excess physisorbed precursor is removed during the subsequent purge step. The optimal length of subsequent nitrogen purging was determined to be 5 s.

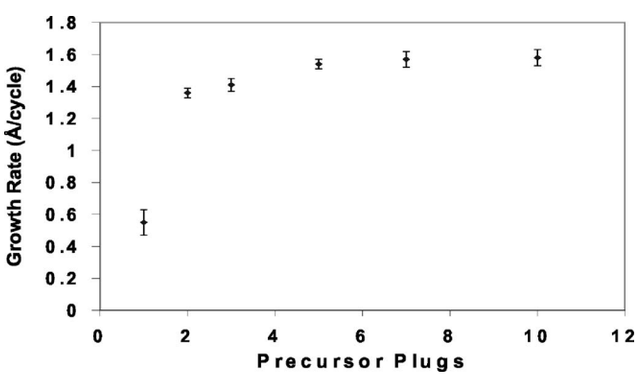

Figure 3. Growth rate (Å/cycle) of aluminum oxide on Si(100) vs number of precursor plugs; the reactor temperature is 400°C. Alumina growth rate appears to saturate to 1.4 Å/cycle at about five plugs.

Temperature.— The deposition rate dependence on reactor temperature is shown in Figure 4 with error bars indicating film uniformity. The temperature of the reactor is measured at the outside surface of the quartz tube within the middle of the heated zone. This data shows the wide temperature window for ALD of aluminum oxide with TDEAA from about 200 to 400°C with no significant change in deposition rate. The film uniformity seems to improve with temperature in this ALD temperature regime. There is a sharp increase in deposition rate at 450°C, which most likely is due to precursor decomposition. In all other data presented here, alumina was deposited at 400°C.

Inert gas purge after the moisture pulse.— In this work, the moisture pulse length was set to 0.05 s, which for ALD represents the shortest pulse time of the computer-controlled manifold system. However, due to the response time of the pneumatic valves, the pulse time is longer than this as there is no difference in deposition growth as moisture pulse is adjusted from 0.05 to 0.8 s. Therefore, in this study excess physisorbed moisture was removed by increasing the nitrogen purge length following the moisture pulse in order to obtain ALD. Figure 5 shows the effect of inert gas purge length following the moisture pulse on the growth rate of ALD alumina. Alumina growth rate decreases with increasing nitrogen purge length until the nitrogen purge duration levels off at about 40 s. This indicates that the 0.05 s moisture pulse saturates the surface with moisture (probably through hydroxylation), and physisorbed moisture along with excess gaseous and surface reaction by-products is

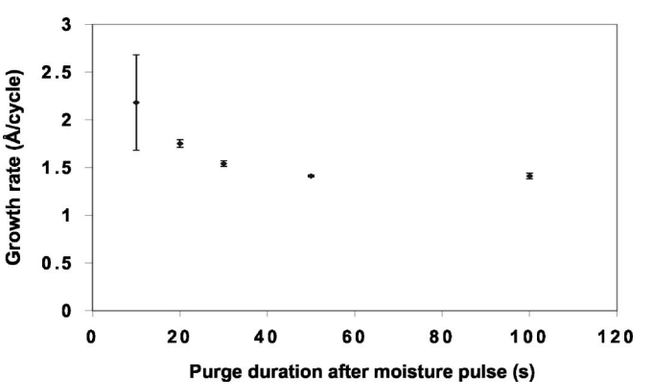

Figure 5. Growth rate (Å/cycle) of aluminum oxide on Si(100) at 400°C reactor temperature, and five plugs vs inert gas purge length following a moisture pulse 0.05 s long. The alumina growth rate appears to saturate to 1.4 Å/cycle at about 40 s inert gas purge.

Downloaded 12 Jul 2008 to 128.248.155.225. Redistribution subject to ECS license or copyright; see http://www.ecsdl.org/terms_use.jsp

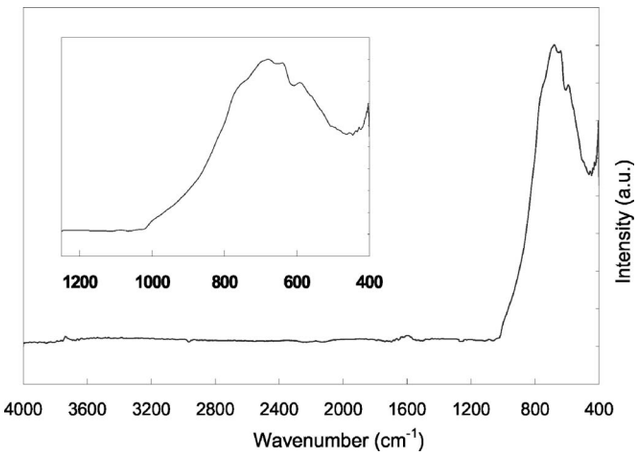

Figure 6. FTIR spectrum of 16 nm thick as-deposited alumina film on Si (with ~1 nm thick silicon oxide after the standard RCA cleaning). The inset shows an exploded view of the 400–1200 cm^{-1} spectral region. Other ALD conditions: 400°C reactor temperature, five plugs of TDEAA precursor followed by 5 s of nitrogen purge, and then 0.05 s of moisture pulse followed by 40 s of nitrogen purge.

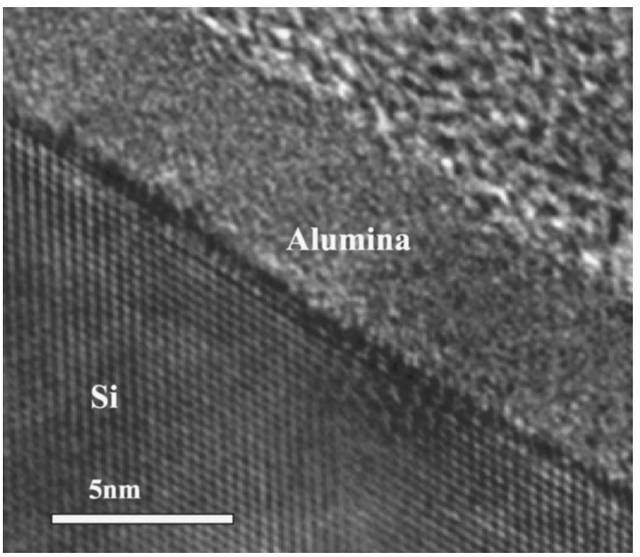

Figure 7. TEM micrograph of as-deposited alumina (5.2 nm thick) on Si deposited under the same conditions as in Fig. 6.

removed after about 40 s of nitrogen purging. The ALD rate at these conditions is about 1.4 Å/cycle. Additional experiments were done with the water pulse set to zero, while everything else was kept the same in our ALD system; in these cases, no deposition was found on the substrate, even after 200–300 pulses of the TDEAA precursor.

Unless stated otherwise, the typical ALD conditions used in this work are five plugs of TDEAA precursor followed by 5 s of nitrogen purging and then 0.05 s of moisture pulse followed by 40 s of nitrogen purge; the ALD temperature is 400°C and the system pressure is 250 mTorr (at the end of the precursor plugs it is lower).

Film and interface characterization: FTIR results.— Figure 6 shows FTIR spectra of aluminum oxide film in the absorbance mode. The fundamental vibrations of solids are localized in the low-frequency region of the IR spectrum (<1200 cm^{-1}).[22] Absence of any Si–O growth during deposition is evident from the lack of Si–O–Si symmetric absorption peak at 1070 cm^{-1}. Lack of any hydrocarbon absorption peaks at ~3000 cm^{-1} and 1600 cm^{-1} indicates negligible organic residue present in as-deposited films. FTIR and XPS analyses show that carbon contamination is below the detection limit of the XPS and FTIR spectrometers (i.e., <1 atom %) in the film. Features due to hydroxyl groups at 3400 cm^{-1} are also absent.[23] Peaks at 640 and 710 cm^{-1} correspond to the O–Al–O bending mode and the Al–O stretching mode, respectively.[24-26] The apparent absence of peak at~530 cm^{-1} due to Al–O stretching in condensed AlO_6 octahedra indicates an amorphous structure of the film.[27] An absorbance peak due to Al = O at 1345 cm^{-1} is also absent.[24] The small peak observed at ~600 cm^{-1} is due to silicon.

STEM/EELS studies.— Figure 7 shows a TEM micrograph of the as-deposited aluminum oxide film on RCA-cleaned Si substrate. The aluminum oxide film appears to be amorphous in the TEM image, which is consistent with the FTIR analysis above, and the Si(100) is easily identified by the crystalline fringes. There is a potential challenge in using TEM micrographs to define the interface of the two amorphous layers, i.e., Al_2O_3 and SiO_2. These two layers appear in different contrast in the micrograph, with silica having the darker contrast. One may expect that the difference in contrast can be used to identify thickness. However, the apparent thickness of the inter-

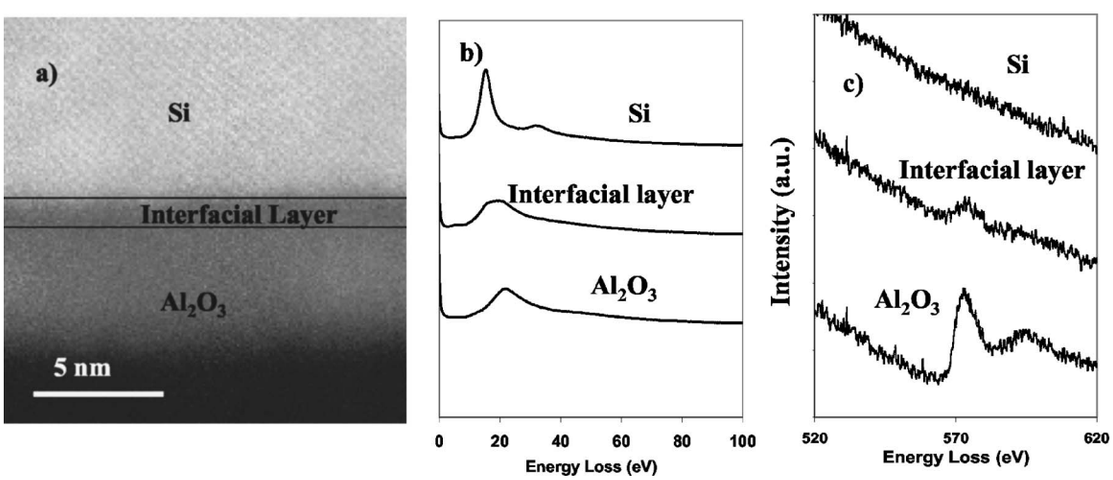

Figure 8. (a) Z-contrast (high-angle ADF) image of alumina (~5.2 nm) on Si(100) substrate deposited at the same conditions as in Fig. 6; (b) low-loss EEL and (c) O K-edge spectra of silicon substrate, interfacial layer, and aluminum oxide.

Downloaded 12 Jul 2008 to 128.248.155.225. Redistribution subject to ECS license or copyright; see http://www.ecsdl.org/terms_use.jsp

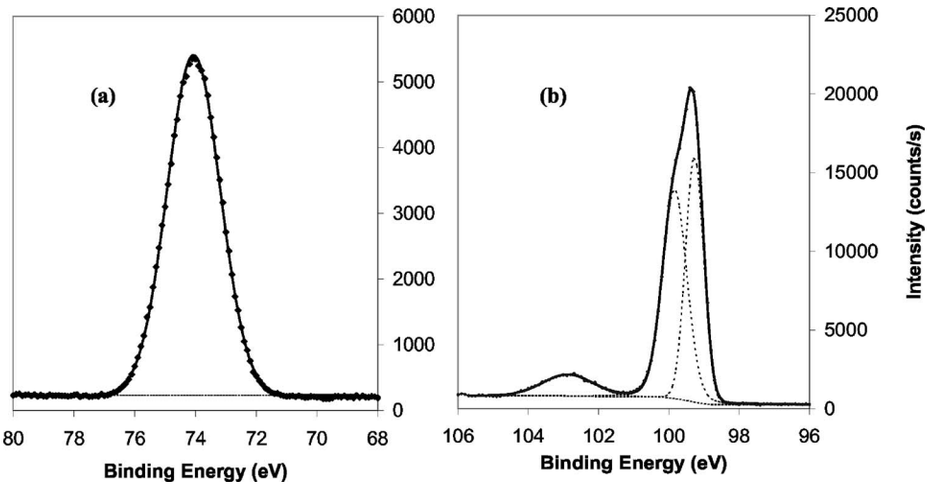

Figure 9. (a) Al 2p and (b) Si 2p core-level spectra of a 4.5 nm thick as-deposited alumina film on Si at 400°C.

facial silica layer changes with change of focus probe and it is difficult to judge the right contrast for defining the true interface.

A more reliable way of determining the film and interfacial layer thickness is to use the Z-contrast image in which films with different atomic number appear in different contrast. For thin samples, the image contrast in high-angled annular dark field (HAADF) is roughly proportional to Z^2 (atomic number).[28] This gives the Z-contrast image good sensitivity even for elements with close atomic numbers like Al (13) and Si (12). In STEM, the atomic-resolution HAADF image is formed by scanning a focused electron beam (a few angstroms in diameter) and collecting the electrons that are elastically scattered to large angles (>50 mrad) on an annular dark field (ADF) detector. Figure 8a shows Z-contrast (high-angle dark field) image of an Al_2O_3/interfacial layer/Si stack. From these measurements, the thickness of the alumina layer is determined to be 52 ± 2 Å and that of the interfacial layer to be 10 ± 2 Å.

Figure 8b shows the EEL spectra in the low-loss region (0–100 eV) of the three distinct regions in the STEM image. EEL spectra in the low-loss region give information about valence electrons of species and it is referred to as valence EELS (VEELS). The bottom spectrum of Figure 8b has a peak at 23 eV which is attributed to aluminum oxide.[29,30] The top spectrum has the characteristic Si signal at 18 eV and a second plasmon at about 35 eV.[31,32] The middle spectrum (Figure 8b) corresponds to the interfacial layer and it has a broad feature at 22 eV. This peak has been attributed to silicon dioxide.[31,32] FTIR analysis revealed no silica growth during aluminum oxide deposition. Therefore, the silica at the interface is the residual native oxide from the standard RCA cleaning procedure used.

Figure 8c shows O K-edge EEL spectra of the three distinct regions in the STEM image. The top spectrum of Fig. 8c corresponds to the silicon substrate and it has no O K-edge features. The middle spectrum of Fig. 8c from the interfacial layer includes a single peak at 570 eV, corresponding to silica, while the bottom spectrum has characteristic O K-edge features of alumina at 570 and 590 eV. These corroborate our low-loss spectra findings that the interfacial layer mainly consists of silicon oxide and the interface with alumina is fairly abrupt.

XPS results.— Figure 9a includes Al 2p core loss spectra of a 4.5 nm thick alumina film deposited on Si at 400°C. This spectrum could not be deconvoluted into more than one symmetric peak at 74.1 eV corresponding to Al^{3+}; this indicates that the film mainly consists of Al_2O_3 and it lacks Al–Al clusters or substoichiometric alumina in the film.[33,34] Figure 9b shows Si 2p core loss spectra of the sample used above for Al 2p spectra. The Si 2p spectra show two main peaks at ~99.3 eV corresponding to bulk Si. The Si 2p peak can be deconvoluted into Si $2p_{3/2}$ (99.3 eV) and Si $2p_{1/2}$ (99.8 eV) features because of the high-energy-resolution capability.[35] There is also a smaller higher binding energy peak at about 102.9 eV. This component at the higher energy results from a higher oxidation chemical state of Si. The separation between bulk Si and Si oxidation state is 3.6–4.0 eV, which suggests the Si^{+4} oxidation state.[33] This indicates the interfacial layer to mainly consist of silicon dioxide. No silicate formation is evidenced.[33]

Conclusions

In this work we introduce a novel, nonpyrophoric, oxygen-free, halogen-free TDEAA precursor for aluminum oxide deposition. We observe the vapor pressure of precursor to increase exponentially with temperature. ALD of aluminum oxide using TDEAA and water was observed to be self-limiting with respect to both reactants with an ALD rate of 1.4 Å/cycle. The temperature window for ALD in the hotwall reactor was found to be between 200 and 400°C. Uniformity was observed to be increasing with temperature even within the ALD regime. At higher temperatures above 400°C there was a significant increase in the growth rate which was attributed to precursor decomposition. FTIR analysis indicates negligible interfacial SiO_2 growth during deposition. Both FTIR spectra and a TEM micrograph show the ALD aluminum oxide to be amorphous. Also, FTIR analyses show no indication of carbon and nitrogen contamination in the film. Z-contrast images and EEL spectra show uniform aluminum oxide film with an abrupt interface with Si. XPS analysis reveals stoichiometric aluminum oxide film on stoichiometric silicon dioxide/Si substrate with no Al–Al cluster formation or silicate formation at the interface of the as-deposited films.

Acknowledgments

The authors are grateful to John Roth, at the Research Resource Center of University of Illinois at Chicago, who provided help with the electron microscope and XPS. The authors are also grateful to Laurent Duquesne at American Air Liquide, Chicago, for help with TDEAA characterization and in setting up the ALD reactor. This research was supported by the NSF-GOALI grant no. 0329195.

University of Illinois at Chicago assisted in meeting the publication costs of this article.

References

1. G. D. Wilk, R. M. Wallace, and J. M. Anthony, *J. Appl. Phys.*, **89**, 5243 (2001).
2. J. Robertson, in *Band Offsets of Wide-bandgap Oxides and Implications for Future Electronic Devices*, p. 1785–1791, AVS, Raleigh, NC (2000).
3. S. Miyazaki, *J. Vac. Sci. Technol. B*, **19**, 2212 (2001).
4. K. J. Hubbard and D. G. Schlom, *J. Mater. Res.*, **11**, 2757 (1996).
5. R. D. Shannon, *J. Appl. Phys.*, **73**, 348 (1993).
6. E. P. Gusev, E. Cartier, D. A. Buchanan, M. Gribelyuk, M. Copel, H. Okorn-Schmidt, and C. D'Emic, *Microelectron. Eng.*, **59**, 341 (2001).
7. K. L. Ng, N. Zhan, C. W. Kok, M. C. Poon, and H. Wong, *Microelectron. Reliab.*,

Downloaded 12 Jul 2008 to 128.248.155.225. Redistribution subject to ECS license or copyright; see http://www.ecsdl.org/terms_use.jsp

43, 1289 (2003).
8. N. Zhan, M. C. Poon, C. W. Kok, K. L. Ng, and H. Wong, *J. Electrochem. Soc.*, **150**, F200 (2003).
9. M.-H. Cho, H. S. Chang, Y. J. Cho, D. W. Moon, K.-H. Min, R. Sinclair, S. K. Kang, D.-H. Ko, J. H. Lee, J. H. Gu, and N. I. Lee, *Surf. Sci.*, **554**, L75 (2004).
10. M.-H Cho, Y. S. Roh, C. N. Whang, K. Jeong, H. J. Choi, S. W. Nam, D.-H. Ko, J. H. Lee, N. I. Lee, and K. Fujihara, *Appl. Phys. Lett.*, **81**, 1071 (2002).
11. M. Ritala and M. Leskela, *Atomic Layer Deposition*, Vol. 1, Academic Press, San Diego, CA (2001).
12. R. Matero, A. Rahtu, M. Ritala, M. Leskela, and T. Sajavaara, *Thin Solid Films*, **368**, 1 (2000).
13. A. W. Ott, K. C. McCarley, J. W. Klaus, J. D. Way, and S. M. George, *Appl. Surf. Sci.*, **107**, 128 (1996).
14. G. S. Higashi and C. G. Fleming, *Appl. Phys. Lett.*, **55**, 1963 (1989).
15. S. M. George, A. W. Ott, and J. W. Klaus, *J. Phys. Chem.*, **100**, 13121 (1996).
16. J. A. Aboaf, *J. Electrochem. Soc.*, **114**, 948 (1967).
17. T. Maruyama and T. Nakai, *Appl. Phys. Lett.*, **58**, 2079 (1991).
18. J. S. Becker, S. Suh, S. Wang, and R. G. Gordon, *Chem. Mater.*, **15**, 2969 (2003).
19. E. M. James and N. D. Browning, *Ultramicroscopy*, **78**, 125 (1999).
20. P. D. Nellist and S. J. Pennycook, *Ultramicroscopy*, **78**, 111 (1999).
21. N. D. Browning, M. F. Chisholm, and S. J. Pennycook, *Nature*, **366**, 143 (1993).
22. C. Morterra and G. Magnacca, *Catal. Today*, **27**, 497 (1996).
23. A. C. Dillon, A. W. Ott, J. D. Way, and S. M. George, *Surf. Sci.*, **322**, 230 (1995).
24. Z. Katz-Tsameret and A. Raveh, in *Characterization of Aluminum-Based Oxide Layers Formed by Microwave Plasma*, pp. 1121–1127, Denver, CO (1995).
25. S.-L. Lin and C.-S. Hwang, *J. Non-Cryst. Solids*, **202**, 61 (1996).
26. A. R. Chowdhuri, C. G. Takoudis, R. F. Klie, and N. D. Browning, *Appl. Phys. Lett.*, **80**, 4241 (2002).
27. P. Tarte, *Spectrochim. Acta, Part A*, **23**, 2127 (1967).
28. B. Foran, J. Barnett, P. S. Lysaght, M. P. Agustin, and S. Stemmer, *J. Electron Spectrosc. Relat. Phenom.*, **143**, 151 (2005).
29. H. Müllejans and R. H. French, *J. Phys. D*, **29**, 1751 (1996).
30. K. Suenaga, D. Bouchet, C. Colliex, A. Thorel, and D. G. Brandon, *J. Eur. Ceram. Soc.*, **18**, 1453 (1998).
31. I. Berbezier, J. M. Martin, C. Bernardi, and J. Derrien, *Appl. Surf. Sci.*, **102**, 417 (1996).
32. C. Gatts, G. Duscher, H. Mullejans, and M. Ruhle, *Ultramicroscopy*, **59**, 229 (1995).
33. T. M. Klein, D. Niu, W. S. Epling, W. Li, D. M. Maher, C. C. Hobbs, R. I. Hegde, I. J. R. Baumvol, and G. N. Parsons, *Appl. Phys. Lett.*, **75**, 4001 (1999).
34. Y.-C. Jung, H. Miura, K. Ohtani, and M. Ishida, *J. Cryst. Growth*, **196**, 88 (1999).
35. W. R. Salaneck, R. Bergman, J.-E. Sundgren, A. Rockett, T. Motooka, and J. E. Greene, *Surf. Sci.*, **198**, 461 (1988).

Downloaded 12 Jul 2008 to 128.248.155.225. Redistribution subject to ECS license or copyright; see http://www.ecsdl.org/terms_use.jsp